

UC Santa Barbara

UC Santa Barbara Previously Published Works

Title

Active tension network model suggests an exotic mechanical state realized in epithelial tissues

Permalink

<https://escholarship.org/uc/item/9qw3z15c>

Journal

Nature Physics, 13(12)

ISSN

1745-2473

Authors

Noll, Nicholas
Mani, Madhav
Heemskerk, Idse
[et al.](#)

Publication Date

2017-12-01

DOI

10.1038/nphys4219

Peer reviewed



Published in final edited form as:

Nat Phys. 2017 December ; 13(12): 1221–1226. doi:10.1038/nphys4219.

Active Tension Network model suggests an exotic mechanical state realized in epithelial tissues

Nicholas Noll¹, Madhav Mani², Idse Heemskerk³, Sebastian J. Streichan^{1,4}, and Boris I. Shraiman^{1,4}

¹Department of Physics, University of California Santa Barbara

²Department of Applied Mathematics, Northwestern University

³Department of Biosciences, Rice University

⁴Kavli Institute for Theoretical Physics

Abstract

Mechanical interactions play a crucial role in epithelial morphogenesis, yet understanding the complex mechanisms through which stress and deformation affect cell behavior remains an open problem. Here we formulate and analyze the Active Tension Network (ATN) model, which assumes that the mechanical balance of cells within a tissue is dominated by cortical tension and introduces tension-dependent active remodeling of the cortex. We find that ATNs exhibit unusual mechanical properties. Specifically, an ATN behaves as a fluid at short times, but at long times supports external tension like a solid. Furthermore, an ATN has an extensively degenerate equilibrium mechanical state associated with a discrete conformal - “isogonal” - deformation of cells. The ATN model predicts a constraint on equilibrium cell geometries, which we demonstrate to approximately hold in certain epithelial tissues. We further show that isogonal modes are observed in the fruit fly embryo, accounting for the striking variability of apical areas of ventral cells and helping understand the early phase of gastrulation. Living matter realizes new and exotic mechanical states, the study of which helps to understand biological phenomena.

Mechanics of growth and cellular rearrangement defines the shape of developing tissues, thereby playing a central role to morphogenesis. It has become a subject of intense study aiming to identify specific mechanical processes involved in cell and tissue-wide dynamics[1–4], uncover the regulatory mechanisms [5], and identify if and how the mechanical state of the tissue feeds back onto the larger developmental program [6–8].

An epithelial tissue is a monolayer of apico-basally polarized cells that are tightly connected to their lateral neighbors. Viewed from their apical sides, cells form an approximately polygonal tiling of the plane. Each cell has a cortical cytoskeleton consisting of actin-myosin

Users may view, print, copy, and download text and data-mine the content in such documents, for the purposes of academic research, subject always to the full Conditions of use: http://www.nature.com/authors/editorial_policies/license.html#terms

Author Contributions

Model formulation and analysis: BIS,IH,MM,NN. Experimental data: SJS. Numerical simulations and data analysis: NN. Manuscript: BIS,NN. All authors discussed the results and implications of the work as well as provided critical comments on the manuscript at all stages.

fibers [9, 10] localized along its perimeter just below the apical surface [11]. A cell's cortical cytoskeleton is linked to those of the neighboring cells via cadherin-mediated adherens junctions [12], resulting in a mechanical network that ensures the integrity of the epithelial layer. The equilibrium geometry of cells is determined by the balance of cytoskeletal and adhesive forces [5] within the tissue. Unlike passive materials, cells actively regulate these forces through mechano-transduction and internal remodeling [13, 14], resulting in an intrinsically dynamic relation between stress and strain, and controllable plasticity, that can drive rearrangement of cells. Elucidating the manner in which cellular activity manifests itself in the collective properties of the tissue is critical to advancing our understanding of morphogenesis.

In this study we formulate a phenomenological model of an epithelial tissue as a two dimensional Active Tension Network (ATN), which in addition to cytoskeletal elasticity describes cytoskeletal re-modelling through myosin activity and dynamic recruitment of myosin to the cytoskeleton, thus capturing the plastic and adaptive response of cells to external stress. We shall explore static and dynamic properties of the ATN model, validate some of its predictions by comparing with live imaging data, and identify new directions of further study.

Formulation of the Active Tension Net Model

Epithelial monolayers can be approximately represented by two-dimensional polygonal tilings, parameterized by a set of vertex coordinates $\{\mathbf{r}_i\}$ and are often described by Vertex Models [2, 15] which assume that the geometry of cells minimizes mechanical energy defined in terms of cell edge lengths ($r_{ij} = |\mathbf{r}_i - \mathbf{r}_j|$) and cell areas (A_α). We shall introduce a generalized class of vertex models by adding internal variables to capture active adaptation of the cytoskeleton. We begin by defining mechanical energy in its differential form [16]

$$dE[\{\mathbf{r}_i\}] = \sum_{\langle i,j \rangle} T_{ij} dr_{ij} + \sum_{\alpha} p_{\alpha} dA_{\alpha} \quad (1)$$

where tension, T_{ij} , defines the change in mechanical energy in response to a change of edge length (dr_{ij}) and the 2D 'apical pressure', p_{α} , defines the response to a change in cortical area (dA_{α}). Tension Nets correspond to the situation where pressure differentials between neighboring cells are negligible so that mechanical balance is dominated by cortical tension. In this limit $p_{\alpha} \approx p_0$ with p_0 controlling the total area of cells, and preventing the collapse of the network under the action of tension.

Vertex dynamics is relaxational and is given by

$$\nu \frac{d}{dt} \mathbf{r}_i = - \partial_{\mathbf{r}_i} E = \sum_{(j)_i} T_{ij} \hat{\mathbf{r}}_{ji} = \sum_{(j)_i} \mathbf{T}_{ij} \quad (2)$$

where $\{j\}_i$ denotes the set of all vertices connected to vertex i , \hat{r}_{ij} is a unit vector in the direction from r_i to r_j , and ν represents the effective friction (e.g. [21]) which determines the timescale of mechanical relaxation. Mechanical equilibrium of a Tension Net is reached when tensions balance, which geometrically means that for each vertex i , the three corresponding tension vectors T_{ij} , T_{ik} , T_{il} form a triangle. Since adjacent vertices share an edge, global tension balance implies that the set of T_{ij} 's defines a triangulation as shown in Fig. 1a,b [17, 18].

Microscopically, each edge in this network represents the mechanically coupled actomyosin bundles of neighboring cells, connected to each other via adherens junctions along the cell-cell interface, as shown schematically in Fig. 2a. Vertices serve as physical barriers to the lateral movement of cadherin clusters and contracting actomyosin bundles [19, 20]. The coupled actomyosin bundles along the cell edge form a natural mechanical unit - an “active edge” in Fig 2a - which carries tension. Edge tension, T_{ij} , depends on the edge length r_{ij} as well as on the intrinsic variables representing the local state of the actomyosin bundle and cadherin-mediated adhesion between cells. Specifically, we assume a simple elastic form, $T_{ij} = K(r_{ij} - \ell_{ij})$, parameterizing the internal state of each interface by an intrinsic “rest length” ℓ_{ij} of the underlying actomyosin filament, itself a dynamical variable governed by

$$\ell_{ij}^{-1} \frac{d}{dt} \ell_{ij} = \tau_\ell^{-1} W\left(\frac{T_{ij}}{m_{ij} a T_s}\right) \quad (3)$$

The generic features of the “walking kernel” $W(x)$, illustrated in Fig. 2b, are based on single-molecule experiments [22, 23]: myosins can walk, contracting the actin bundle, unless the load per myosin, T_{ij}/am_{ij} , reaches the “stall force” level T_s , above which the filament elongates as motors slip backwards [24]. Here m_{ij} is the average myosin line-density along the edge and a is the length scale over which motors share mechanical load.

Eqs. (2, 3) define the dynamics of a Tension Net with a specified myosin distribution on interfaces. The fixed point of these equations is reached when i) tensions balance at all vertices and ii) all edges are at their stall tension, set by the local myosin (linear) density ($T_{ij} = aT_s m_{ij}$). Global tension balance requires the set of T_{ij} 's to form a triangulation and therefore edge tensions, and hence myosin levels, cannot be prescribed independently. How can mechanical equilibrium be achieved? At this point we recall that myosin distribution within tissues is not fixed and is known to respond to mechanical cues [8, 25], although the exact form of this mechanical feedback is not fully understood. Here we propose a particular form of mechanical feedback on myosin, that will ensure convergence to a balanced state. The latter is achieved if myosin recruitment depends on the internal strain rate of each filament:

$$m_{ij}^{-1} \frac{d}{dt} m_{ij} = \alpha \ell_{ij}^{-1} \frac{d\ell_{ij}}{dt} \quad (4)$$

with α parameterizing the rate of myosin recruitment, which we assume to be slow relative to both mechanical relaxation and actomyosin contractility. This form of mechanical feedback recruits myosin to overloaded slipping bundles and reduces myosin on unloaded contracting bundles until the stall condition is reached, bringing the system to equilibrium. The “Dynamic Recruitment” hypothesis, defined by Eq (4), is dictated by the requirement of ATN stability and should be regarded as a prediction of the model to be tested by future experiments.

Equilibrium Manifold of a Tension Net

The ‘duality’ between an equilibrium tension net and the corresponding triangulation of the tension plane (see Fig. 1ab) implies the existence of certain constraints on cell geometry. Let $\theta_{i\beta}$ be the angle at vertex i belonging to cell β ; its complement $\pi - \theta_{i\beta}$ is the corresponding angle of the dual triangle in the tension plane (Fig. 1ab). By applying the law of sines to the triangles surrounding dual vertex a one discovers the following constraint, true for every cell:

$$\chi_\alpha = \prod_{i \in \mathcal{V}_\alpha} \frac{\sin \theta_{i\gamma}}{\sin \theta_{i\beta}} = 1 \quad (5)$$

The product is taken over the set \mathcal{V}_α of vertices i that belong to cell α , while β and γ label other cells adjacent to i in clockwise order (Fig. 1a, see the SI for a full derivation). An array with all $\chi_\alpha = 1$ is geometrically *compatible* with tension-balance. Since χ_α can be readily measured, the compatibility constraint allows one to quantitatively assess whether a given cell array is consistent with a balanced tension net.

The geometry of the dual triangulation also constrains possible sets of balanced tensions. A triangulation is specified by the positions of its c (the number of polygonal cells in the array) vertices, and hence has $2c$ independent degrees of freedom. This number is smaller than the number of edges $e = 3c$ (assuming all vertices in the cell array are three-fold), which means that T_{ij} 's can't be prescribed independently: the balanced set satisfies c constraints.

The above counting argument further implies that the map between cell geometry and tension triangulation is highly degenerate. The number of degrees of freedom of a compatible cell array is given by $2v - c = 3c$ (v being the number of vertices of the cell array), which is c degrees of freedom larger than that of the dual triangulation. Hence, a given set of balanced tensions corresponds to a manifold of nets with one degree of freedom per cell. Specifically, as long as none of the vertex angles are perturbed, we can freely “inflate” or “deflate” cells, as illustrated in Fig. 3a, with no cost of energy and thus without disturbing mechanical equilibrium and the underlying tension triangulation. Quite generally such angle preserving - hereafter referred to as “isogonal” deformations have the form

$$\delta \mathbf{r}_i = S_{\alpha\beta\gamma}^{-1} [\mathbf{T}_{ij} \Theta_\beta + \mathbf{T}_{ik} \Theta_\alpha + \mathbf{T}_{il} \Theta_\gamma] \quad (6)$$

where δr_i denotes the displacement of vertex i shared by cells α, β, γ and $S_{\alpha\beta\gamma}$ (Fig. 1ab) is the area of the vertex's dual triangle. $\{\Theta_\alpha\}$ parameterize the c -dimensional manifold of equilibrium states. Tensions $\{\mathbf{T}_{ij}, \mathbf{T}_{ik}, \mathbf{T}_{il}\}$ capture the implicit geometric constraints within tension nets central to the structure of the isogonal modes: note for example that $\delta r_i = 0$ for $\Theta_\alpha = \Theta_\beta = \Theta_\gamma$. The compatibility condition (see Eq. 5) satisfied by equilibrium tension nets is essential for allowing such isogonal modes to exist. Because they do not invoke a restoring force, isogonal deformations are easily excitable “soft modes” and are expected to dominate observed fluctuations of tension nets close to mechanical equilibrium. We note that isogonal modes can be thought of as a discrete manifestation of the conformal symmetry that appears in 2D continuum elasticity in the limit of a vanishing bulk modulus (see SI for details). Isogonal modes also generalize the isoperimetric “breathing modes” of a hexagonal lattice [26].

Dynamical properties of Active Tension Nets

Let us consider the dynamics of small perturbations around a mechanical equilibrium state, which can be described by linearizing Eqs. (2–4). While detailed calculations are carried out in the SI, the key features can be understood from a vastly simpler analysis of a 1D “Active Tension Chain” model which has the form

$$\frac{d}{dt}\delta T_n = D\nabla^2\delta T_n - \kappa(\delta T_n - \delta m_n) \quad (7)$$

$$\frac{d}{dt}\delta m_n = \bar{\alpha}(\delta T_n - \delta m_n) \quad (8)$$

where δT_n and δm_n are deviations from the equilibrium state and n is an integer indexing edges along the chain (note that we have rescaled δm_n with $T_s a$ to give it the units of tension). $\nabla^2\delta T_n = \delta T_{n+1} + \delta T_{n-1} - 2\delta T_n$ is the discrete Laplacian in 1D and $\{D, \kappa, \bar{\alpha}\}$ are parameters derived (in the SI) by linearization of Eqs. (2–4). Eq. 7 is recognized as the Maxwell model of viscoelasticity forced by myosin perturbations δm_n . A static local forcing δm_0 (in Eq. 7) would generate a persistent flow (i.e. non-zero rate of strain) and exponentially localized perturbations of tension with “screening length” $\lambda = \sqrt{D/\kappa}$. At long times myosin recruitment, Eq. 8, (with $\bar{\alpha} \ll \kappa$) ensures that the chain converges towards mechanical equilibrium $\delta m_n = \delta T_n = T_B$ where T_B is external tension at the boundaries. Relaxation towards this equilibrium is governed by $\frac{d}{dt}\delta m_n \approx \bar{\alpha}\kappa^{-1}D\nabla^2\delta T_n$ and

$\frac{d}{dt}\delta r_n \approx \bar{\alpha}\kappa^{-1}D\nabla^2\delta T_n$ where $\frac{d}{dt}\delta r_n$ is the deformation rate of edge n . Hence despite the ATN's viscoelastic response and floppy modes at short times, the long time behavior is effectively elastic with $K_{eff} \sim \bar{\alpha}\kappa^{-1}D$. An analogous crossover from fluid-like response at intermediate times to solid-like behavior at long times occurs in the fully two-dimensional ATN (see Fig. 3cd).

ATN predictions and the Ventral Furrow (VF) formation in *Drosophila* embryo

One of the striking predictions of the ATN model is the existence of the isogonal soft modes that allow easy variability of cell area. Extreme variability of apical cell area has been observed at the beginning of the gastrulation process in *Drosophila*, when cells along the ventral midline of the embryo constrict their apical surfaces, initiating the formation of a furrow that subsequently internalizes the future mesoderm [27], as shown in Fig. 4ab. This apical constriction was shown to be driven by pulsed contractions of the *medial* actomyosin network (located near the apical cell surface) that pull on the *cortical* cytoskeleton. The process has been described as a “ratchet” [28]: medial myosin pulses cause transient constrictions subsequently stabilized by the retracted cytoskeletal cortex.

Here, we propose an alternative interpretation of the phenomenon in terms of the ATN model. If we assume that the *cortical* myosin concentrations are relatively static over the timescale of medial myosin pulsing, the ATN model predicts that any transient perturbation of mechanical balance due to medial myosin contractions would leave behind an isogonal deformation of the cell array, as it returns to mechanical balance dominated by cortical tensions that remain unchanged. Hence we predict that cell deformation during the early stages of ventral furrow formation should be well described by motion along an isogonal manifold.

The proposed model is predicated on the applicability of the tension net hypothesis that underlies the ATN model. While it is not yet possible to measure all internal tensions in a living tissue, Eqn. 5 provides us with a quantitative assay of the validity of the balanced tension net approximation in the ventral furrow using apical geometry alone. Exact satisfaction of the constraint $\log \chi = 0$ is not anticipated owing to the errors associated with the acquisition and analyses of imaging data, as well as due to cell array fluctuations that result in deviations from tension balance. Yet even if tension-balance is only approximate, we expect that the empirical $\log \chi$ distribution would be closer to zero than the “control distribution” computed for a random cell array (see the SI for details). Fig. 4d presents the result of such an analysis for the VF. Based on ~ 5000 cells, we find a statistically significant (Kolmogorov-Smirnov [29] $p < 10^{-9}$) accumulation of $\log \chi$ near zero with respect to the null – consistent with an approximate tension balance within the tissue. This finding is non-trivial, as results of the same analysis for *Drosophila* larval wing imaginal disc [30], Fig. 4e, yielded no statistically significant tendency towards $\log \chi \approx 0$. See the SI for further discussion of the statistical test and the analysis of other tissues.

We further quantified the early VF formation process using time-lapse imaging of fluorescently-labelled myosin and cell membranes (see Methods). Relative levels of cortical myosin (excluding an overall magnitude increase [28] that does not affect local tension balance) and edge orientations do not change significantly over the course of VF formation, despite large changes in edge lengths (Fig. 4c). This finding, together with the approximate “compatibility” of embryonic mesoderm (Fig. 4d), lend strong support to the validity of the assumptions underlying the ATN model interpretation of the VF formation process in terms of isogonal deformations driven by transient medial myosin pulses.

Analyzing five movies of VF formation (as in Fig 4ab) we found that isogonal deformations r^{iso} , found by least squares analysis of Eq. 6, consistently account for ~85% of the measured vertex displacements, Fig. 4g (see SI for more details). The spatial profile of $\{\Theta_a\}$, integrated over the course of VF dynamics is approximately parabolic (see Fig. 4f), giving rise to isogonal, but anisotropic, constriction of cells with the long axis of cells oriented along the anterior-posterior direction [27]. Thus, the mesoderm during VF formation indeed appears to behave as a transiently perturbed ATN, owing along the isogonal manifold comprised of the degenerate set of its (mechanical) equilibrium states (see Fig. 3b). The ATN model provides a reduced set of degrees of freedom that accurately describe the dynamics of VF formation.

Finally we discuss the phenotypes of *twist* and *snail* mutants [28]. *snail* embryos fail to coalesce medial myosin structures and do not initiate pulsed contraction of cells [28]; hence *snail* embryos simply lack the transient perturbations necessary to induce isogonal “flow” along the equilibrium manifold. Conversely, *twist* embryos exhibit pulsed apical contraction of cells but are unable to fully stabilize the constricted state [28]. These mutants also appear to have reduced tension in the cortical cytoskeleton and exhibit strongly curved cell-cell interfaces. The latter fact suggests relatively large differences in pressures between adjacent cells, in which case contribution of pressure to local force balance cannot be neglected. Pressure variation lifts the degeneracy of the ATN mechanical equilibrium manifold so that isogonal deformations experience a restoring force, thus limiting the response to transient perturbations (see the SI for an extended discussion).

“Dynamic Recruitment” hypothesis

The ATN model presented in this study describes epithelial tissue dynamics in terms of three processes: i) fast relaxation towards mechanical equilibrium dominated by cortical tension, ii) myosin driven rearrangements of the cortex on an intermediate time scale, and iii) on the slowest timescale, Dynamic Recruitment (or reduction) of myosin that is driven by the internal *rate of strain* in the cortex, Eq. (4). The first two alone would result in a viscoelastic fluid behavior (driven by myosin generated internal forces). The unusual behavior arises from the assumed Dynamic Recruitment of myosin, which dramatically changes the asymptotic behavior so that while being able to flow at short times, ATNs, like solids, can support external stress at long times. While the presented measurements suggest the validity of tension-balance in describing the mechanical equilibrium of an epithelial tissue, new experiments will be needed to test the Dynamic Recruitment hypothesis, which was introduced to explain how myosin levels at different interfaces can be coordinated to attain tension balance across a tissue.

Materials and Methods

The following fly stocks were used for ventral furrow live recordings: Spider-GFP [32], sqh-GFP;membrane-mCherry [31]. Embryos were dechorionated following standard protocols, and mounted in Matek Dishes for imaging. Images were acquired on a Leica SP8 confocal, with a 40x/N.A. 1.1 objective water immersion objective. See SI for details on image analysis and numerical simulation of ATN dynamics.

The data that support the figures and other findings of this study, as well as the MATLAB code used to perform simulations of ATN dynamics, are available from the corresponding author upon request.

Supplementary Material

Refer to Web version on PubMed Central for supplementary material.

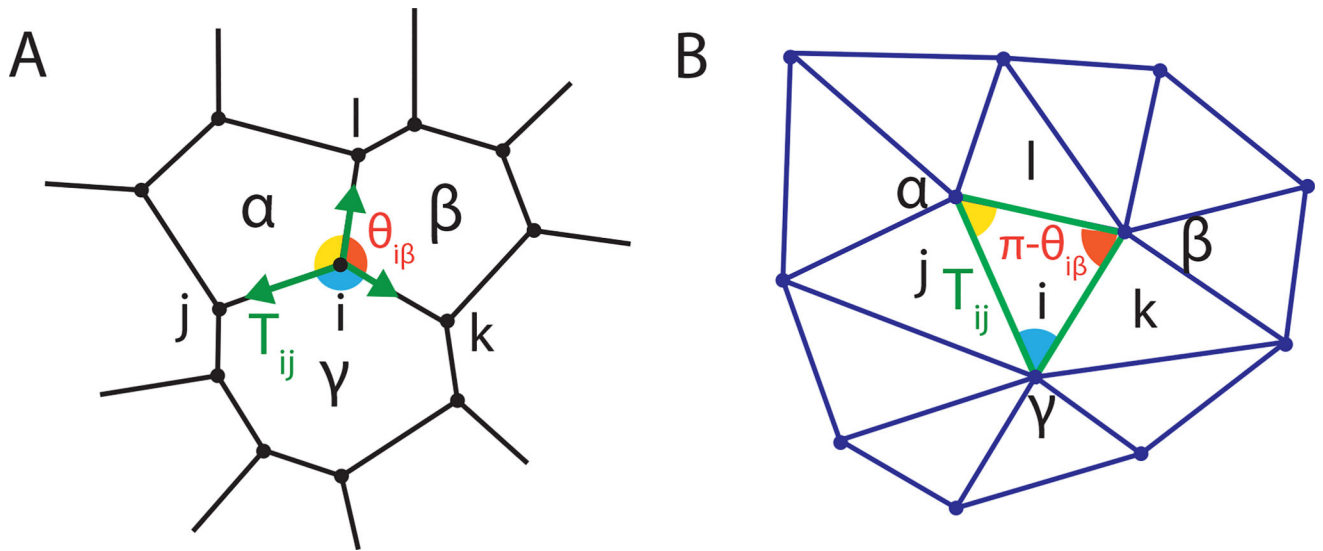
Acknowledgments

The authors gratefully acknowledge stimulating discussions with Ken Irvine, Thomas Lecuit, and Eric Wieschaus and thank K. Irvine for sharing the wing imaginal disc data. This work was supported by the NSF PHY-1220616 (BIS,NN) and PHY-1125915 (MM), GBMF grant #2919 (BIS/IH) and NICHD 5K99HD088708-02 (SJS).

References

1. Bellaiche Y, Heisenberg C. Forces in Tissue Morphogenesis and Patterning. *Cell*. 153(5):948–962.2013; [PubMed: 23706734]
2. Farhadifar R, Roper JC, Aigouy B, Eaton S, Julicher F. The influence of cell mechanics, cell-cell interactions, and the proliferation of epithelial packing. *Current Biology*. 17(24):2095–2104.2007; [PubMed: 18082406]
3. Rauzi M, Verant P, Lecuit T, Lenne PF. Nature and anisotropy of cortical forces orienting *Drosophila* tissue morphogenesis. *Nature Cell Biol*. 10:1401–1410.2008; [PubMed: 18978783]
4. He B, Doubrovinski K, Polyakov O, Wieschaus E. Apical constriction drives tissue-scale hydrodynamic flow to mediate cell elongation. *Nature*. 508:392–396.2014; [PubMed: 24590071]
5. Lecuit T, Lenne PF. Cell surface mechanics and the control of cell shape, tissue patterns, and morphogenesis. *Nat. Rev. Mov. Cell Biol*. 8:633–644.2007;
6. Nelson C, Jean R, Tan J, Liu W, Sniadecki N, Spector A, Chen C, et al. Emergent patterns of growth controlled by multicellular form and mechanics. *Proc. Natl. Acad. Sci. U. S. A.* 102(33):11594–11599.2005;
7. Shraiman B. Mechanical feedback as a possible regulator of tissue growth. *Proc. Natl. Acad. Sci. U. S. A.* 102(9):3318–3323.2005; [PubMed: 15728365]
8. Fernandez-Gonzalez R, Simeos M, Roper JC, Eaton S, Zallen J. Myosin II dynamics are regulated by tension in intercalating cells. *Dev. Cell*. 17(5):736–43.2009; [PubMed: 19879198]
9. MacKintosh FC, Levine AJ. Nonequilibrium Mechanics and Dynamics of Motor-Activated Gels. *Phys. Rev. Lett.* 100(1):018104.2008; [PubMed: 18232824]
10. Wang N, et al. Cell prestress. I. Stiffness and prestress are closely associated in adherent contractile cells. *Am J Physiol - Cell Physiol*. 282(3):606–16.2002;
11. Salbreux G, Charras G, Paluch E. Actin cortex mechanics and cellular morphogenesis. *Cell*. 152(10):536–545.2012;
12. Hartsock A, Nelson WJ. Adherens and Tight Junctions: Structure, Function and Connections to the Actin Cytoskeleton. *Biochim Biophys Acta*. 1778(3):660–669.2008;
13. Wozniak M, Chen C. Mechanotransduction in development: a growing role for contractility. *Nat. Rev. Mov. Cell Biol*. 10:34–43.2009;
14. Kasza K, Rowat A, Liu J, Angelini T, Brangwynne C, Koenderink G, Weitz D. The cell as a material. *Current Opinion in Cell Biology*. 19(1):101–107.2007; [PubMed: 17174543]
15. Honda H. Geometric models for cells in tissues. *International Review for Cytology*. 81:191–248.1983;
16. Chiou K, Hufnagel L, Shraiman B. Mechanical stress inference for two dimensional cell arrays. *PLOS Comp. Bio*. 8(5):e1002512.2012;
17. Maxwell JC. Relaxing in foam. *Phil. Mag.* 27:250.1864;
18. Henkes S, O'Hern CS, Chakraborty B. Entropy and Temperature of a Static Granular Assembly: An Ab Initio Approach. *Phys. Rev. Lett.* 99:038002.2007; [PubMed: 17678329]

19. Choi W, et al. Remodeling the zonula adherens in response to tension and the role of afadin in this response. *J. Cell Biol.* 213(2):243–260.2016; [PubMed: 27114502]
20. Cavey M, Lecuit T. Molecular Bases of Cell-Cell Junctions Stability and Dynamics. *Cold Spring Harb. Persp. Bio.* 1(5):a002998.2009;
21. Marchetti MC, Joanny JF, Ramaswamy S, Liverpool TB, Prost J, Rao M, Simha R. Hydrodynamics of soft active matter. *Rev. Mo. Phys.* 85(3):1144–1189.2013;
22. Clemen A, et al. Force-dependent stepping kinetics of myosin-V. *Biophys J.* 88(6):4402–4410.2005; [PubMed: 15764664]
23. Norstrom M, Smithback PA, Rock R. Unconventional processive mechanics of non-muscle myosin IIB. *J Biol. Chem.* 285(34):26326–26334.2010; [PubMed: 20511646]
24. Kolomeisky AB, Fisher M. Molecular motors: a theorist’s perspective. *Annu. Rev. Phys. Chem.* 58:675–695.2007; [PubMed: 17163836]
25. Pouille PA, Ahmadi P, Brunet AC, Farge E. Mechanical signals trigger myosin II redistribution and mesoderm invagination in *Drosophila* embryos. *Sci. Signal.* 2:ra16.2009; [PubMed: 19366994]
26. Villain, J. Two-Dimensional Solids and Their Interaction with Substrates. In: Riste, T, editor *Ordering in strongly fluctuating condensed matter systems*. Plenum; New York: 1980. 221
27. Sweeton D, Parks S, Costa M, Wieschaus E. Gastrulation in *Drosophila*: the formation of the ventral furrow and posterior midgut invaginations. *Development.* 112(3):775–89.1991; [PubMed: 1935689]
28. Martin AC, Kaschube M, Wieschaus E. Pulsed contractions of an actin-myosin network drive apical constriction. *Nature.* 457(7228):495–9.2009; [PubMed: 19029882]
29. Massey F Jr. The Kolmogorov-Smirnov Test for Goodness of Fit. *J Amer. Statist. Assoc.* 46:68–78.1951;
30. Rauskolb C, et al. Cytoskeletal Tension Inhibits Hippo Signaling through an Ajuba-Warts Complex. *Cell.* 158:143–156.2014; [PubMed: 24995985]
31. Martin AC, Gelbart M, Fernandez-Gonzalez R, Kaschube M, Wieschaus E. Integration of contractile forces during tissue invagination. *J. Cell. Biol.* 188:735749.2010;
32. Morin X, Daneman R, Zavortink M, Chia W. A protein trap strategy to detect GFP-tagged proteins expressed in their endogenous loci in *Drosophila*. *Proc. Natl. Acad. Sci. U. S. A.* 98(26):15050–15055.2002;

**FIG. 1.**

Force balance in a tension net defines a triangulation of the “tension plane”. (A) 2D array of cells represented by a polygonal tiling. In mechanical equilibrium tensions balance at each vertex. (B) Equilibrated tensions form a triangulation, with triangle angles supplementary to the angles at the corresponding vertex.

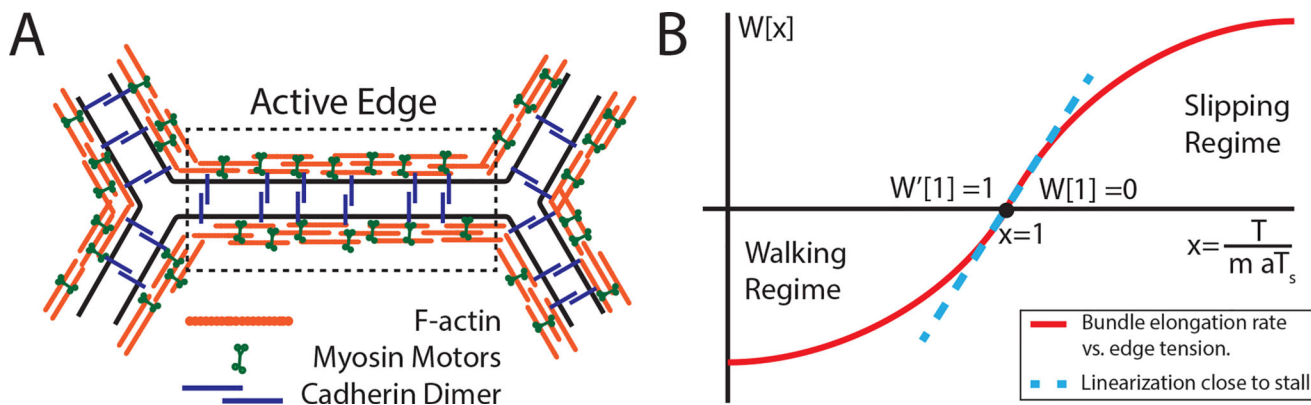


FIG. 2. Role of myosin motors in the ATN model. (A) Schematic of the basic active element of a tension network: actomyosin cables on apposing interfaces are cross-linked by cadherin dimers; (B) Dependence of the actomyosin bundle contraction rate on mechanical load: the “walking kernel” $W(x)$, see Eq. (3), changes sign from contraction to elongation when mechanical load per myosin T/am exceed the stall load T_s .

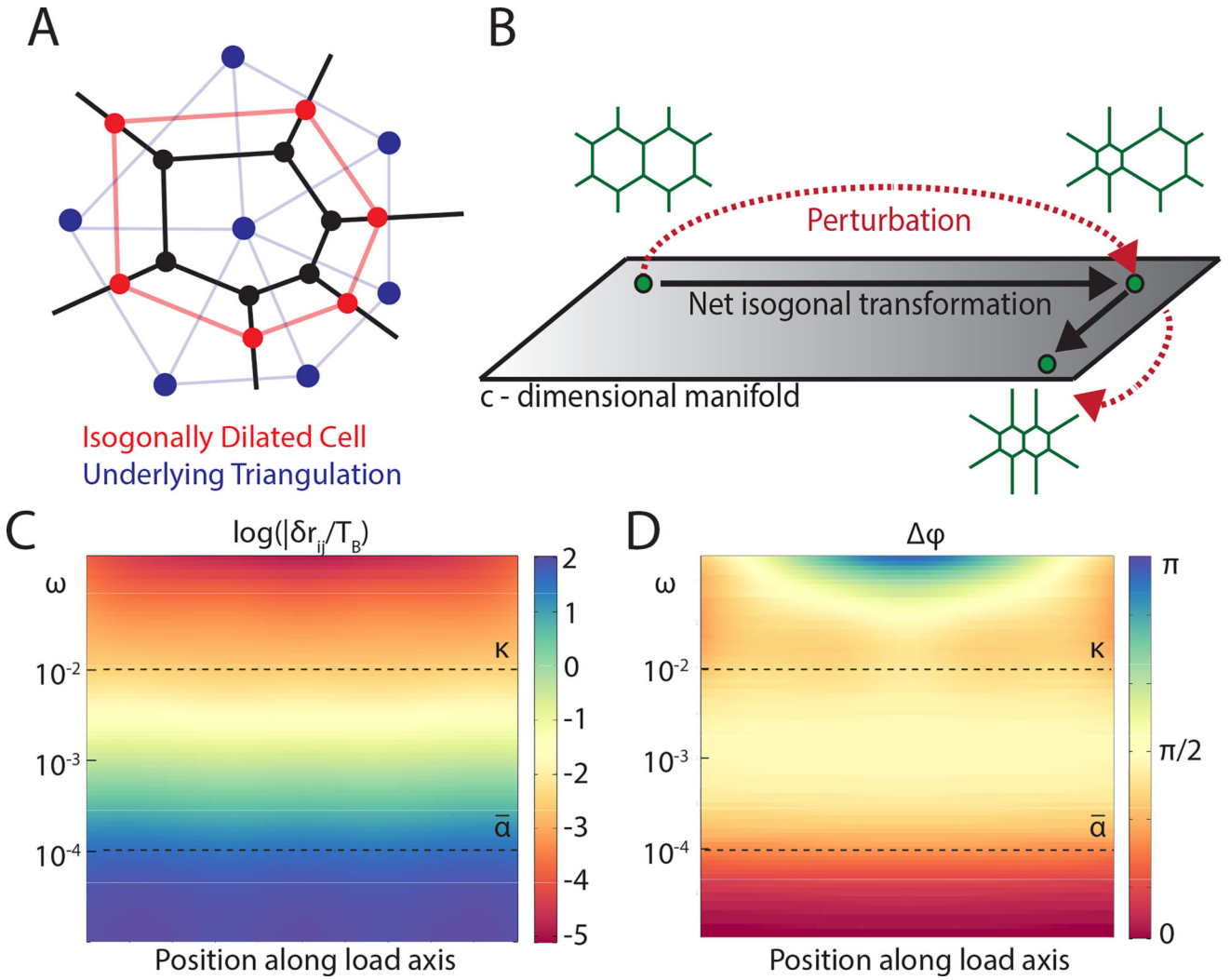


FIG. 3. Mechanical properties of an ATN. (A) Cartoon of an *isogonal* ‘breathing mode’ of a cell in a tension net. (B) Because ATN equilibrium is a manifold rather than a point, after a transient perturbation the system does not necessarily return to the same state, resulting in an ‘isogonal’ transformation. (C) Amplitude and (D) phase of the longitudinal strain (as a function of position) in response to periodic uniaxial forcing $T_B \cos \omega t$ applied at the boundaries ($\kappa = 10^{-2}$ and $\bar{a} = 10^{-4}$). As the frequency ω decreases below \bar{a} the phase shifts from $\pi/2$ to 0 indicating crossover from viscous fluid behavior to an elastic solid. This contrasts with the conventional Maxwellian viscoelasticity crossover towards elasticity with ω increasing above κ (see SI for details).

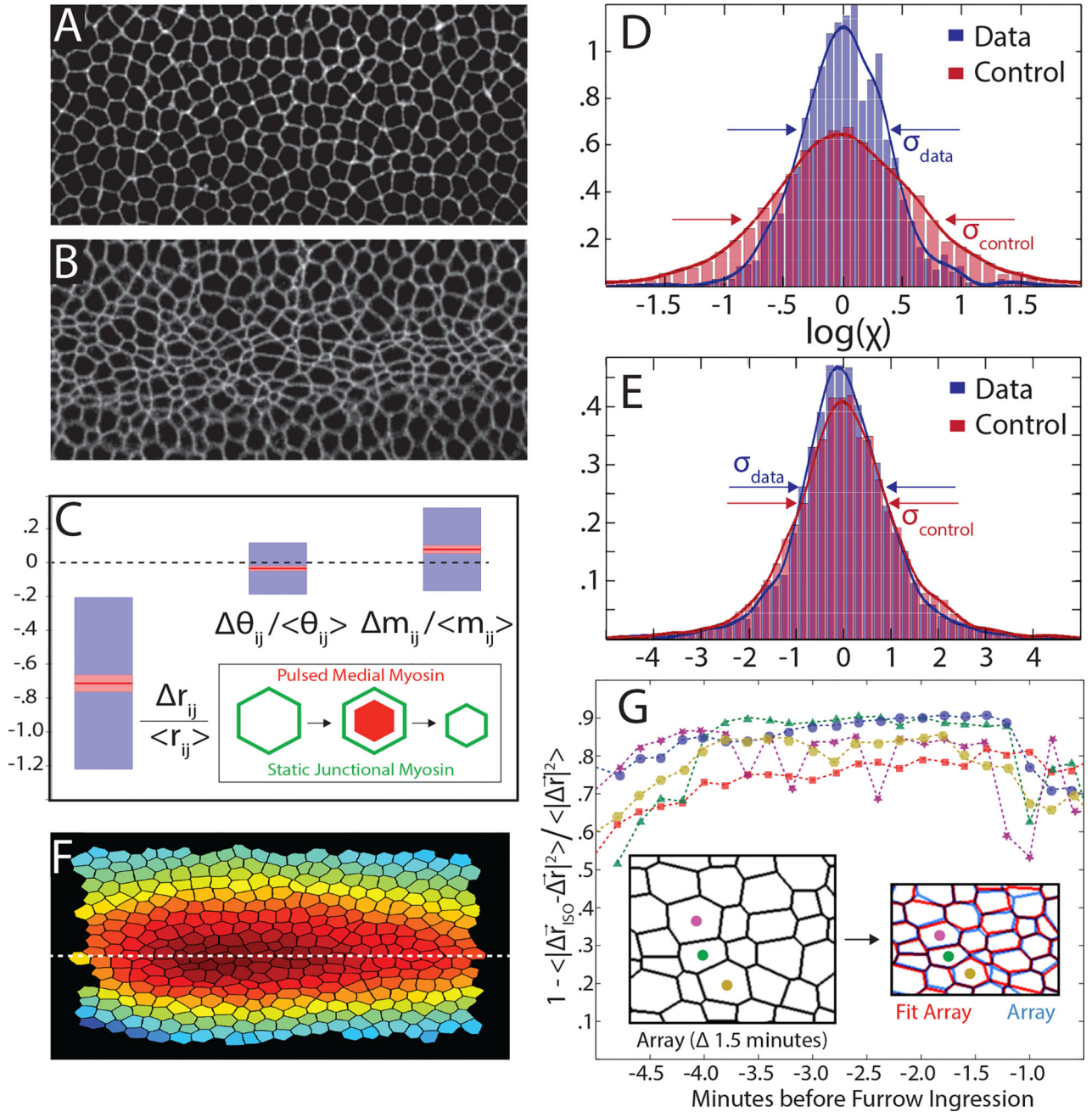


FIG. 4. Experimental tests of ATN model predictions. (A–B) Ventral view of *Drosophila* embryo (imaged using Spider-GFP marking cell membranes) at the beginning of VF formation (A) and 4 minutes later (B). Note the variability of apical cell area in (B). (C) The measured changes in edge length r_{ij} , edge orientation angle θ_{ij} and relative myosin level m_{ij} during VF formation: red lines denote the means (with pink haloes giving 95% confidence intervals on the mean given by the t-test) and blue boxes denote one standard deviation. Edge length shrinks by $\sim 75\%$ while relative changes in cortical myosin and edge orientation are considerably smaller. (D–E) Test of compatibility (Eq.5) compares the PDF of the

measured $\log \chi$'s (blue) with the control distribution (red) defined by permuting angles. Embryonic mesoderm (D) exhibits a strong tendency towards compatibility ($\log \chi \approx 0$) while epithelium of the third instar imaginal wing disc (E), does not. (F) Spatial profile of the isogonal mode amplitude, $\{\Theta_\alpha\}$ describes increasing anisotropic compression of cells towards ventral midline. (G) Fraction of measured deformation (r) captured by isogonal deformation (r_{iso}) obtained via least squares minimization of Eq.6. Each color represents an independent measurement with 200 cells. Inset: a graphical comparison for a sample fit.